Available online at www.sciencedirect.com
ScienceDirect
Catalysis Today 136 (2008) 146–155
CATALYSIS TODAY
www.elsevier.com/locate/cattod

Influence of ceria on the NO_x storage/reduction behavior of lean NO_x trap catalysts

Yaying Ji [a], Jae-Soon Choi [b], Todd J. Toops [b], Mark Crocker [a,*], Mojghan Naseri [c,1]

[a] *Center for Applied Energy Research, University of Kentucky, 2540 Research Park Drive, Lexington, KY 40511-8479, USA*
[b] *Fuels, Engines and Emissions Research Center, Oak Ridge National Laboratory, 2360 Cherahala Boulevard, Knoxville, TN 37932-1563, USA*
[c] *DCL International Inc., P.O. Box 90, Concord, Ontario, Canada L4K 1B2*

Available online 22 January 2008

Abstract

The effect of La_2O_3-stabilized ceria incorporation on the functioning of fully formulated lean NO_x trap catalysts was investigated. Monolithic catalysts were prepared, corresponding to loadings of 0, 50 and 100 g CeO_2/L, together with a catalyst containing 100 g/L of ceria–zirconia ($Ce_{0.7}Zr_{0.3}O_2$). Loadings of the other main components (Pt, Rh and BaO) were held constant. Catalyst evaluation was performed on a bench flow reactor under simulated diesel exhaust conditions, employing NO_x storage/reduction cycles. NO_x storage efficiency in the temperature range 150–350 °C was observed to increase with ceria loading, resulting in higher NO_x conversion levels. At 150 °C, high rich phase NO_x slip was observed for all of the catalysts, resulting from an imbalance in the rates of nitrate decomposition and NO_x reduction. Optimal NO_x conversion was obtained in the range 250–350 °C for all the catalysts, while at 450 °C high rich phase NO_x slip from the most highly loaded ceria-containing catalyst resulted in lower NO_x conversion than for the ceria-free formulation. N_2O was the major NO_x reduction product at 150 °C over all of the catalysts, although low NO_x conversion levels limited the N_2O yield. At higher temperatures N_2 was the main product of NO_x reduction, although NH_3 formation was also observed. Selectivity to NH_3 decreased with increasing ceria loading, indicating that NH_3 is consumed by reaction with stored oxygen in the rear of the catalyst.

Keywords: NO_x; Storage; Reduction; LNT; Ceria

1. Introduction

Lean-burn engines provide more efficient fuel combustion and lower CO_2 emissions compared with traditional stoichiometric engines. However, the effective removal of NO_x from lean exhaust represents a challenge to the automotive industry. In this context, Lean NO_x Traps (LNTs) represent a promising technology. Although many studies have been conducted using model $Pt/BaO/Al_2O_3$ type LNT catalysts, to date there have been relatively few reports concerning the effect of ceria on LNT performance [1–8], and of these, several deal with the role of ceria as a support for the main BaO NO_x storage phase [3–5]. In addition to its role as a potential support material, ceria possesses a number of other functions in LNT catalysis. In the case of LNTs formulated for lean-burn gasoline applications, its role is principally to provide the necessary oxygen storage capacity when the engine is operating at the stoichiometric point (i.e., the catalyst is functioning as a conventional three-way catalyst) [9]. However, ceria also promotes H_2 formation under rich conditions via the water-gas shift (WGS) reaction [10,11], which can be expected to facilitate catalyst regeneration and desulfation [1].

Recent studies have also shown that ceria possesses significant NO_x storage capacity [8,12–16], particularly at low to moderate temperatures (<400 °C). This finding is of particular significance for diesel engine applications, given that exhaust gas temperatures of diesel engines are typically lower than those of lean-burn gasoline engines. While exhaust gas temperatures are engine dependent and vary with the relationship between engine size and vehicle mass, in the case of the FTP-75 cycle, for example, effective NO_x reduction catalysts for light duty diesel applications would need to have peak

* Corresponding author. Tel.: +1 859 257 0295; fax: +1 859 257 0302.
E-mail address: crocker@caer.uky.edu (M. Crocker).
[1] Present address: Johnson Matthey Inc., 380 Lapp Road, Malvern, PA 19355, USA.

0920-5861/$ – see front matter © 2007 Elsevier B.V. All rights reserved.
doi:10.1016/j.cattod.2007.11.059

performance in the range 200–300 °C [17]. Ceria-containing LNT catalysts are thus interesting candidates for diesel exhaust after treatment, even allowing for the fact that during rich purges oxygen stored by the ceria reacts with the reductants, increasing the total amount of reductant required for LNT regeneration. Indeed, Honda [18] has recently disclosed a two-layer lean NO_x catalyst for diesel engines which is comprised of a ceria-rich LNT catalyst bottom layer and a SCR-type catalyst top layer (SCR, selective catalytic reduction). The bottom layer acts as a NO_x storage catalyst under lean conditions; under rich conditions, the stored NO_x is reduced to NH_3, which is then stored in the top layer where it is available for reaction with NO_x under lean conditions.

In order to gain a better understanding of the benefits and disadvantages of ceria in LNT catalysis, we have previously studied the effect of ceria addition to a model powder catalyst [8]. The presence of ceria was found to improve the NO_x storage capacity in the temperature range 200–400 °C under both continuous lean and lean–rich cycling conditions. Furthermore, temperature-programmed experiments showed that NO_x stored in the ceria-containing catalyst was thermally less stable and more reactive to reduction with both H_2 and CO as reductants. In view of these benefits, we have extended our studies to model catalysts which are more representative of fully formulated LNT catalysts. In this paper, we report the results of a study conducted on monolithic catalysts in which the loading of ceria was varied. For comparison purposes, a catalyst containing a commercial ceria–zirconia material was also included in the study.

2. Experimental

2.1. Catalyst preparation

Catalysts were prepared according to the following method:

(a) $Pt(NH_3)_4(OH)_2$ and $Rh(NO_3)_3$ were co-impregnated onto a 3 wt.% La_2O_3-stabilized γ-alumina (Sasol Puralox SCFa-140 L3, BET surface area of 140 m^2/g) to give a loading of 2.35 wt.% Pt and 2.35 wt.% Rh after calcination at 500 °C for 2 h.
(b) γ-Alumina (Sasol Puralox SCFa-140 L3) was impregnated with $Ba(O_2CCH_3)_2$ to give a loading of 21 wt.% BaO after calcination at 500 °C for 2 h.
(c) The BaO/Al_2O_3 material from above (140 g/L washcoat) was ball milled with the required amount of 5 wt.% La_2O_3-stabilized CeO_2 powder (Advanced Material Resources, BET surface area of 119 m^2/g) or CeO_2–ZrO_2 (Actalys 9800 from Rhodia, Ce/Zr = 70/30, BET surface area of 114 m^2/g). To achieve the total Pt loading of 3.53 g/L, the balance of the Pt (equivalent to 2.83 g/L washcoat) was then impregnated onto the mixture (as $Pt(NH_3)_4(OH)_2$), after which it was calcined at 500 °C for 2 h.
(d) The powder prepared in step (a), in an amount corresponding to 30 g/L washcoat, was then mixed with the powder from (c), balance La_2O_3-stabilized γ-alumina was added and the resulting mixture was slurried in water (30–40 wt.% solids content). A small amount of boehmite sol (ca. 6 g/L washcoat) was added as a binder, after which the slurry was washcoated onto 4″ × 6″ cordierite 400 cpsi/6.5 mil monoliths and calcined at 550 °C for 2 h.

Each of the above impregnations was performed according to the incipient wetness method. To minimize experimental variability between the preparations, one batch each of powders (a) and (b) was prepared for use in the different preparations. The quantities of ceria, ceria–zirconia and balance alumina powders were adjusted to give the component loadings shown in Table 1. The total washcoat loading was 260 g/L. Washcoating was performed by DCL International Inc. (Toronto, ON) using a proprietary vacuum coating process.

2.2. Catalyst characterization

Surface area and pore volume measurements were performed according to the BET method by nitrogen adsorption at −196 °C using a Micromeritics Tri-Star system. Prior to the measurements catalyst samples (washcoat and monolith) were ground to a fine powder and outgassed overnight at 160 °C under vacuum. High resolution transmission electron microscopy (HRTEM) measurements were carried out with a JEOL 2010 FasTEM field emission electron microscope operated at an accelerating voltage of 200 kV. The point-to-point resolution of the electron beam was 0.3 nm.

2.3. Catalyst evaluation

Catalyst evaluation was performed on a bench flow reactor. A 2.1 cm diameter and 7.4 cm long core taken from each LNT monolith was wrapped in Zetex insulation tape and inserted into a horizontal quartz reactor tube (2.2 cm internal diameter). The reactor tube was heated by an electric furnace, and simulated exhaust gas mixtures were introduced from pressurized gas bottles (ultra high purity grade, Air Liquide). The gases were metered with mass flow controllers (Unit Instruments Series 7300, Kinetics Electronics) and pre-heated before entering the quartz reactor. Water was introduced by a peristaltic cartridge pump (Cole-Parmer) to a heated zone, vaporized and added to the simulated exhaust mixture.

A rapid switching four-way valve system was used to alternate between the lean and rich gas mixtures so that the

Table 1
Composition of prepared catalysts

Component	Catalyst code/loading[a]			
	30–0	30–50	30–100	30–100 Z
Pt (g/L; g/cuft)	3.53 (100)	3.53 (100)	3.53 (100)	3.53 (100)
Rh (g/L; g/cuft)	0.71 (20)	0.71 (20)	0.71 (20)	0.71 (20)
BaO (g/L)	30	30	30	30
CeO_2[b] (g/L)	0	50	100	0
CeO_2–ZrO_2 (g/L)	0	0	0	100
Al_2O_3[c] (g/L)	Balance	Balance	Balance	Balance

[a] Nominal loadings. Total washcoat loading = 260 g/L.
[b] Stabilized with 5 wt.% La_2O_3.
[c] Stabilized with 3 wt.% La_2O_3.

lean/rich/lean transitions in these experiments were almost instantaneous (within 0.2 s). Three K-type thermocouples were placed just before the LNT, at the LNT mid-point and just after the LNT to monitor the temperature profiles. The gas composition was analyzed in situ either at the reactor outlet or inside the reactor/catalyst. At the reactor outlet (or inlet by using a bypass gas line), two heated chemiluminescence detectors (California Analytical Instruments, 400-HCLD) measured NO and NO_x ($NO + NO_2$) concentrations and an FT-IR gas analyzer (Midac M2000) measured NO_2, N_2O, NH_3, CO, CO_2 and H_2O. Intra-catalyst hydrogen measurement was performed by using SpaciMS (Spatially Resolved Capillary Inlet Mass Spectrometer) developed in the Fuels, Engines, and Emissions Research Center at Oak Ridge National Laboratory [19–22]. The mass spectrometer, equipped with a magnetic-sector mass filter, allowed quantitative measurement of H_2 ($m/z = 2$). A minimally invasive capillary inlet system (sampling rate = ca. 10 μL min^{-1}, probe size = ca. 150 μm outer diameter) was employed to transport time-varying species pools to the mass spectrometer for analysis. A capillary probe was introduced from the reactor inlet near the centerline and positioned at different catalyst locations: just before the catalyst inlet, one-quarter of the way into the catalyst, halfway into the catalyst, and just after the catalyst outlet.

After installation, each core sample was degreened at 500 °C for 5 h under lean/rich cycling conditions to establish a consistent initial surface condition. The cycling conditions were identical to those used for NO_x storage/reduction performance evaluation shown in Table 2 except for the temperature (500 °C) and reductant concentration (2.125% CO + 1.275% H_2). Before catalyst evaluation, ''dynamic'' catalyst oxygen storage capacity (OSC) was evaluated at 350 °C under lean/rich cycling conditions (see Table 2) employing the SpaciMS to obtain spatiotemporal H_2 profiles. Given that the feed contained CO_2 and H_2O, it is likely that the reverse water-gas shift (RWGS) reaction occurred during the OSC measurements. It should be noted, however, that if H_2 is consumed via RWGS, the resulting CO can also be consumed by reaction with stored oxygen (with the same stoichiometry), in which case the OSC measurement is correct. The OSC measurement is only incorrect if the formed CO is not consumed and exits the catalyst. CO production measured during the rich phase was, in fact, found to be negligible—hence the reported OSC results are considered accurate.

During the cycling conditions described in Table 2, the observed catalyst breakthrough profiles stabilized to a fixed limit cycle in about 2 h, at which point it was possible to characterize the performance in terms of the 'stationary' concentration cycles. For the determination of product selectivities, N_2O and NH_3 were quantified using the FT-IR analyzer, the selectivity to N_2 being determined by difference (i.e., $S_{N_2} = 100\% - S_{N_2O} - S_{NH_3}$).

Table 2
Gas compositions used for oxygen storage/reduction and NO_x storage/reduction cycling experiments

Parameter	Oxygen storage/reduction cycling		NO_x storage/reduction cycling	
	Lean	Rich	Lean	Rich
Duration (s)	60	5	60	5
Temperature (°C)	350	350	150–450	150–450
Space velocity (h^{-1})	30,000	30,000	30,000	30,000
NO (ppm)	0	0	300	0
O_2 (%)	10	0	10	0
H_2 (%)	0	4.2	0	1.575
CO (%)	0	0	0	2.625
H_2O (%)	5	5	5	5
CO_2 (%)	5	5	5	5
N_2 (%)	Balance	Balance	Balance	Balance

3. Results and discussion

3.1. Catalyst preparation and characterization

As shown in Table 1, four catalysts were prepared, corresponding to loadings of 0, 50 and 100 g CeO_2/L, with the fourth catalyst containing 100 g/L of $Ce_{0.7}Zr_{0.3}O_2$. The loadings of the other components were fixed with the exception of the balance alumina which was used to bring the total washcoat loading up to a value of 260 g/L in each case. The various component loadings, together with the range of ceria loadings employed, were chosen so as to reflect typical commercial catalyst compositions. Catalysts are denoted in this paper by the BaO loading (fixed at 30 g/L) followed by the CeO_2 or $Ce_{0.7}Zr_{0.3}O_2$ loading (the latter indicated by the suffix ''Z''). It should be noted that in these catalysts the BaO/Al_2O_3 and ceria-containing powders were incorporated as a physical mixture, rather than the BaO being supported on the ceria phase. The latter option would have made it impossible to draw a fair comparison between the ceria-containing catalysts and catalyst 30–0 ($Pt/Rh/BaO/Al_2O_3$), given that the BaO phases in the catalysts could be expected to possess different chemical and/or physical properties.

Table 3 shows the results of N_2 physisorption measurements performed on the catalysts. The total surface areas of the samples are low due to the inclusion of the cordierite substrate; however, based on the washcoat loading, and assuming a surface area of 0.5 m^2/g for the cordierite and a substrate density of 435 g/L (manufacturer's data), the surface area of the washcoat can be estimated. These are found to span a fairly narrow range, a consequence of the fact that the surface areas of the Al_2O_3, CeO_2 and $Ce_{0.7}Zr_{0.3}O_2$ powders used in their preparation are similar (see Section 2).

Table 3
Physical properties of prepared catalysts

Catalyst	Estimated washcoat BET surface area (m^2/g)	Total BET surface area (m^2/g)	Pore volume (cm^3/g)	Av. pore radius (nm)
30–0	121	43.5	0.148	6.82
30–50	126	47.5	0.156	6.56
30–100	106	41.9	0.133	6.35
30–100 Z	140	54.7	0.176	6.4

Transmission electron microscopy (TEM) was used to check the precious metal dispersions in the powders used for preparation of the catalysts (the use of H_2 chemisorption being complicated by the fact that these are bimetallic formulations, in addition to the presence of the reducible oxides in some of the powders). The resulting TEM data (Fig. 1) indicated the presence of highly dispersed metal particles. For the Pt–Rh/Al_2O_3 powder used in step (a) of the catalyst preparations, together with the powder prepared in step (c) for the preparation of catalyst 30–0, TEM indicated a narrow particle size distribution with an average metal particle size in the range 2–3 nm. TEM analysis of the powders prepared in step (c) for the preparation of catalysts 30–100 and 30–100 Z (not shown) afforded similar results. Therefore, the precious metal dispersion can be assumed to be rather constant for all the catalysts evaluated in this study.

3.2. Oxygen storage capacity measurements

The catalysts were further characterized on the basis of their oxygen storage properties. For this purpose the catalysts were cycled between lean and rich conditions using the conditions shown in Table 2, while the H_2 concentration at the catalyst outlet was monitored (Fig. 2). An increase in the H_2 breakthrough time is indicative of increasing H_2 consumption by stored oxygen, as is a decrease in the maximum H_2 concentration measured. Based on the quantity of H_2 consumed by each catalyst, the corresponding OSC was calculated. As shown in Fig. 2, the measured OSC increases with ceria loading in the catalyst, with the catalyst containing the $Ce_{0.7}Zr_{0.3}O_2$ mixed oxide (catalyst 30–100 Z) showing the highest OSC, as expected [23]. Based on the measured OSC for 30–100 Z, CO and H_2 concentrations were chosen for subsequent NO_x storage-reduction experiments (Table 2) which were calculated to be just sufficient to fully consume the stored oxygen in this catalyst.

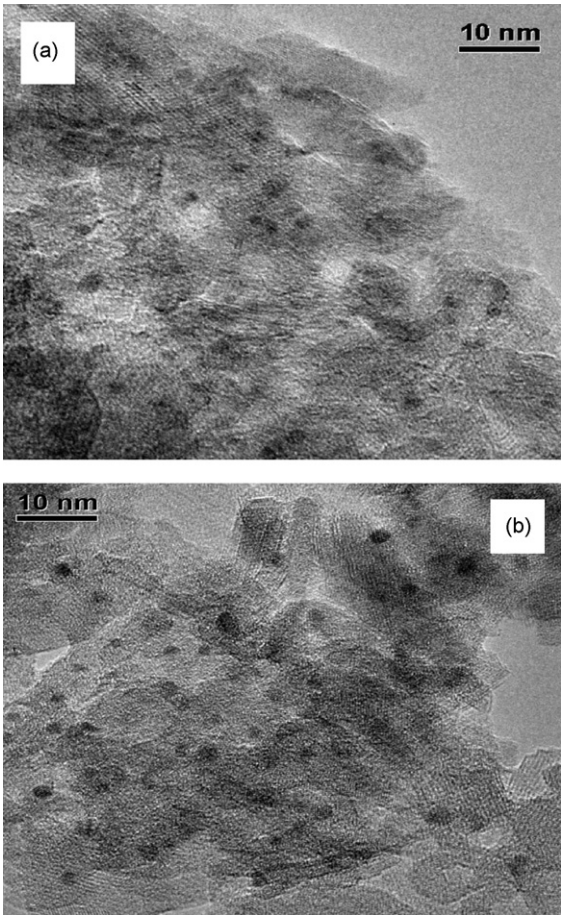

Fig. 1. HRTEM images of powders used for preparation of monolithic catalysts. (a) Pt–Rh/Al_2O_3 (step (a) for all catalysts); (b) Pt/BaO/Al_2O_3 (step (c) for catalyst 30–0).

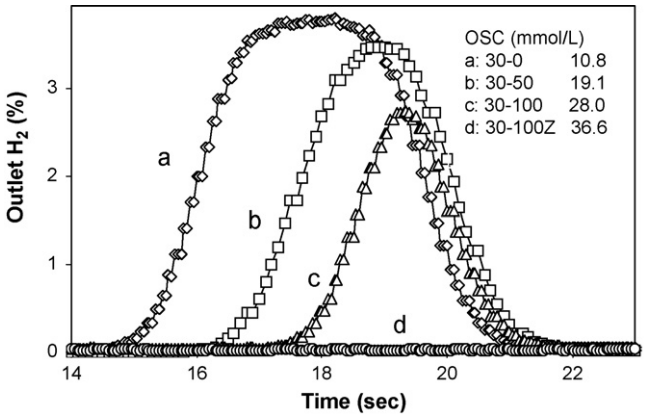

Fig. 2. Measured outlet hydrogen concentration profiles under oxygen storage cycling condition (inlet H_2 concentration = 4.2%).

3.3. NO_x storage and release

NO_x storage and release were investigated under steady state cycling conditions in the range 150–450 °C. As shown in Fig. 3, all of the catalysts exhibited significant lean phase NO_x slip at both low (150 °C) and high (450 °C) temperature. This contrasts with the almost insignificant lean NO_x breakthrough observed at 250 and 350 °C for the catalysts. Compared to the ceria-free catalyst (30–0), the addition of ceria clearly improved NO_x storage performance, with lower lean phase NO_x slip being observed at all temperatures for the ceria-containing catalysts. Table 4 provides an overview of the NO_x storage and release during the cycling experiments. 30–0 displayed a storage efficiency of only ~20% at 150 °C, whereas after incorporating ceria into the catalyst, the storage efficiency improved to 35% for 30–50 and 56% for 30–100 at 150 °C. These findings are consistent with our previous study using powder catalysts [8], in which the presence of ceria was found to improve NO_x storage capacity in the temperature range 200–400 °C.

Given that at 150 °C NO_2 was slipped during the storage phase for all the catalysts (see Table 4), we conclude that the NO_x storage capacity at 150 °C was not limited by the kinetics of NO oxidation. Although the kinetics of nitrate/nitrite formation may be a limiting factor, we suggest that it is mainly the inability to remove nitrates and nitrites at low temperature during the regeneration phase that limits the lean phase NO_x

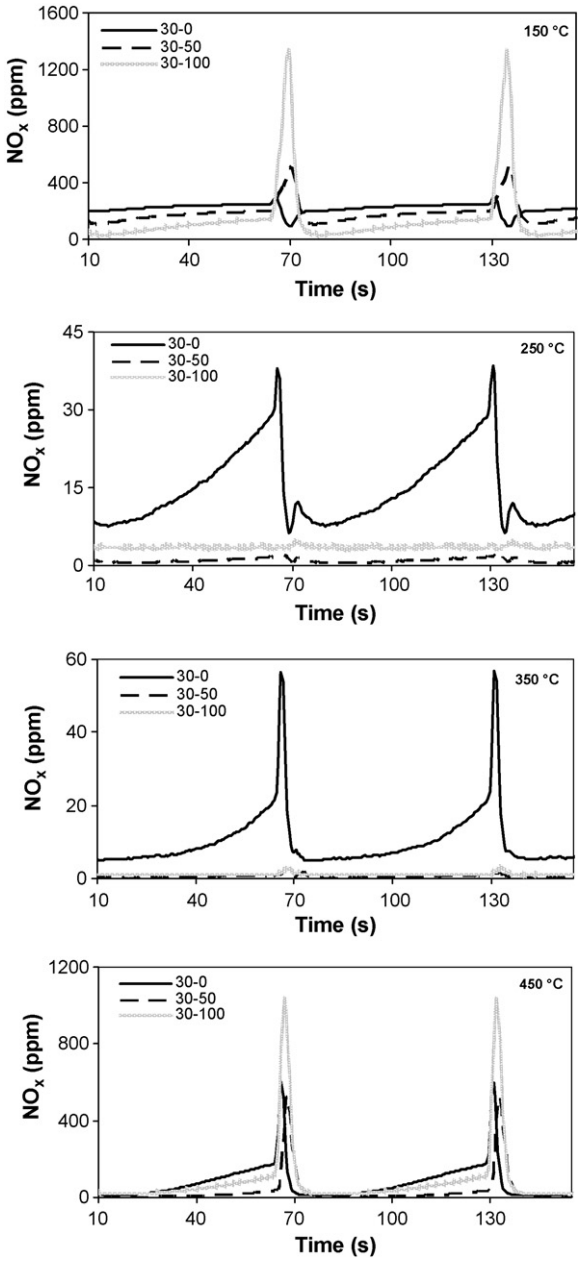

Fig. 3. Comparison of NO_x storage and release for catalysts 30–0, 30–50 and 30–100 during NO_x storage/reduction cycling.

storage efficiency. This is a consequence of the fact that under cycling conditions NO_x storage efficiency represents the product of the intrinsic storage efficiency (i.e., as measured for the first cycle of a ''clean'' catalyst) and the rich phase regeneration efficiency. In this respect, the superior NO_x storage efficiency (and overall NO_x conversion efficiency) observed for the ceria-containing catalysts at 150 °C may be due to more facile decomposition of the nitrates/nitrites present. This is supported by the results of our previous study with powder catalysts [8], in which temperature-programmed experiments showed that NO_x stored in a ceria-containing LNT catalyst was thermally less stable and more reactive to reduction with both H_2 and CO than its ceria-free analog.

With increasing temperature, a storage efficiency greater than 95% was observed for all the catalysts (250–350 °C). However, a further temperature increase up to 450 °C resulted in a dramatic drop in NO_x storage. This can be explained on the basis of the reduced thermal stability of nitrates at high temperatures. We have previously reported a DRIFTS study of Pt/CeO_2 [13] in which it was found that surface nitrates are largely stable to 300 °C upon heating in inert atmosphere, but completely disappear upon heating to 400 °C. In a separate experiment under flowing NO/O_2, nitrate bands were observed at 400 °C, although with greatly reduced intensity relative to the spectrum obtained at 300 °C. Evidently the NO_x storage capacity of ceria is greatly diminished at 400 °C, whereas at lower temperatures it can contribute significantly to the NO_x storage capacity of LNT catalysts. Additionally, a published study concerning the thermal decomposition of nitrates formed by NO_2 storage on $BaO/\gamma\text{-}Al_2O_3$ has reported the occurrence of two main decomposition events, exhibiting differential thermogravimetric (DTG) maxima at 422 and 529 °C (at the same BaO loading as used in this work) [24]. Hence the NO_x storage capacity of $BaO/\gamma\text{-}Al_2O_3$ is also diminished at 450 °C relative to the lower temperatures examined in this work.

With respect to the regeneration behavior of the catalysts, it is apparent that temperature also plays a crucial role in the NO_x release behavior. Of particular note is the pronounced NO_x release displayed by catalyst 30–100 at both low and high temperatures. As shown in Fig. 3, NO_x release reached maximum concentrations of 1300 and 1000 ppm at 150 and 450 °C, respectively, greatly exceeding the commanded feed gas level of 300 ppm. In contrast, 30–100, along with 30–50 and 30–100 Z (not shown), displayed minimal NO_x release at 250 and 350 °C. In the case of 30–0, significant NO_x release was observed at all temperatures, although at 150 °C it was noticeably lower than for the ceria-containing catalysts.

The purge NO_x release results detailed in Table 4 show that 10.9 μmol of the stored NO_x was released from catalyst 30–0 at 150 °C without being reduced, corresponding to 31% of the NO_x stored. The total amount of rich phase NO_x released at this temperature increased with ceria loading, with 30–100 showing the greatest release (36.1 μmol NO_x), representing 37% of the stored NO_x. As highlighted by Epling et al. [25], rich phase NO_x release is dependent on the rates of four processes: reductant delivery, nitrate decomposition, OSC consumption and NO_x reduction. From this it follows that for a given set of conditions it is important to establish a balance between nitrate decomposition and NO_x reduction in order to establish optimum regeneration efficiency. In our study, the high NO_x slip observed for all the catalysts at 150 °C can be ascribed to an imbalance between the rates of nitrate decomposition and NO_x reduction, i.e., the rate of NO_x reduction was too slow for the liberated NO_x to be fully consumed. The fact the ceria-loaded catalysts displayed much higher NO_x release at 150 °C can be attributed largely to their intrinsically higher NO_x storage capacity, due to the ability of ceria to capture NO_x.

Based on the results in Table 4, it can be inferred that while both the nitrate decomposition and NO_x reduction rates increased with increasing temperature, the balance between

Table 4
Comparison of NO_x storage and release during NO_x storage/reduction cycling[a]

Catalyst	Temperature (°C)	Lean-phase NO_x and NO_2 slip (μmol)		Storage efficiency (%)	Rich-phase NO_x release		Averaged lean/rich cycle NO_x conv. (%)
		NO_x	NO_2		μmol	%[b]	
30–0	150	136.6	61.3	20.3	10.9	31.2	14.0
	250	9.1	5.4	94.7	1.1	0.7	94.1
	350	5.5	1.6	96.8	1.6	1.0	95.9
	450	40.9	9.8	76.2	15.2	11.6	67.3
30–50	150	111.1	52.5	35.2	16.7	27.7	25.5
	250	0.6	0.4	99.7	0.1	0.1	99.6
	350	0.3	0.1	99.8	0.1	0.0	99.8
	450	10.0	4.5	94.2	14.9	9.2	85.5
30–100	150	74.7	17.8	56.5	36.1	37.3	35.4
	250	2.1	0	98.8	0.2	0.1	98.7
	350	0.7	0.1	99.6	0.1	0.1	99.6
	450	30.2	6.5	82.4	33.9	24.0	62.6
30–100 Z	150	119.9	25.5	30.1	14.3	27.7	21.8
	250	5.1	1.2	97.0	0.9	0.5	96.5
	350	4.0	0.8	97.7	0.5	0.3	97.4
	450	41.7	0	75.7	13.6	10.5	67.7

[a] Conditions as given in Table 2. The total amount of input NO per lean/rich cycle was 171.5 μmol.
[b] (NO_x released in rich purge/NO_x stored in lean phase) × 100%.

the two was sufficiently improved for the NO_x to be fully reduced at 250 and 350 °C, with almost no NO_x slip. However, at 450 °C, the thermal instability of the nitrates was such that the rate of nitrate decomposition was not fully balanced by the rate of NO_x reduction, resulting in some degree of NO_x slip. In the case of the ceria-containing catalysts, this situation may be exacerbated by the higher exotherms generated in the catalyst during the reaction of the reductants with oxygen stored in the ceria. Although ceria reduction is itself endothermic [26], reaction of the reductants with released oxygen is exothermic, rendering the overall process slightly exothermic. As the local surface is heated, NO_x is released in order to bring the level of NO_x storage down to the maximum amount that can be stored at the higher temperature [27]. Measured mid-bed catalyst temperatures indicated an exotherm of ca. 35 °C for catalyst 30–100 Z (at an inlet temperature of 450 °C), decreasing to 12 °C for 30–0 (Fig. 4). As shown in Table 4, while catalyst 30–100 exhibits a slightly higher lean phase NO_x storage efficiency than 30–0 at 450 °C, the rich phase NO_x release from 30–100 is substantially higher, resulting in a lower overall NO_x conversion (62.6% versus 67.3%). Additionally, we cannot rule out the possibility that for catalysts 30–100 and 30–100 Z, the high OSC of these catalysts may have resulted in localized reductant shortages, thereby contributing to the higher rich phase NO_x release. Although the quantity of reductant used was in principle sufficient for complete consumption of the stored oxygen for 30–100 Z (having the highest OSC), localized shortages of reductant may occur at the reaction front, particularly towards the rear of the catalyst (at which point most of the reductant in the leading edge would have been consumed).

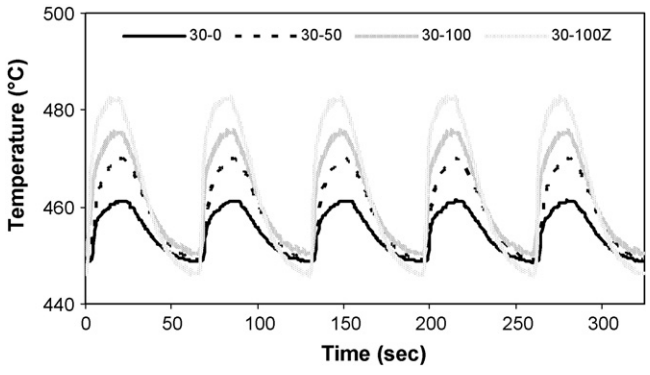

Fig. 4. Temperature profiles at mid-point of catalyst core during NO_x storage/reduction cycling (inlet temperature = ca. 450 °C).

Combining the NO_x storage and reduction performance, Table 4 shows that optimal NO_x conversion is obtained in the range 250–350 °C for all the catalysts. The addition of ceria improved NO_x conversion in the range 150–350 °C, especially at low temperature. We note that similar findings have been reported by Theis et al. [1]; in their work, NO_x conversion at 300 °C was found to be highest for catalysts containing high loadings of cerium-containing mixed oxides due to the correspondingly high NO_x storage capacity. They similarly found that while high ceria loadings are beneficial in this respect, the use of such high loadings results in decreased NO_x conversion at increased temperatures (400–500 °C).

Finally, it is worth noting that catalyst 30–100 was found to display superior NO_x conversion to 30–100 Z at temperatures in the range 150–350 °C. This is in large part due to the lower NO_x storage efficiency displayed by 30–100 Z, and suggests that the $Pt/Ce_{0.7}Zr_{0.3}O_2$ component in 30–100 Z possesses an intrinsically lower NO_x storage capacity than the Pt/CeO_2 in 30–100. This is not unreasonable, given that the Ce–Zr mixed oxide can be expected to be less basic than the La-stabilized ceria [16].

3.4. NO_x reduction

Product selectivity to N_2, N_2O and NH_3 was examined during NO_x reduction under NO_x storage/reduction cycling conditions. As shown in Fig. 5, at 150 °C N_2O is the dominant reduction product for all four catalysts, with 30–0 showing slightly higher selectivity to N_2O than the ceria-containing catalysts. Fig. 6 shows the evolution of N_2O from catalysts 30–0, 30–50 30–100, and 30–100 Z during cycling. As the temperature was increased selectivity to N_2O decreased markedly, such that at 350 and 450 °C only trace amounts of N_2O were detected, with no correlation observed between selectivity to N_2O and catalyst ceria content. Note that due to the slow response time of the FT-IR analyzer, the inherent time resolution of the data is significantly longer than the 5 s duration of the rich phase. Consequently, it proved impossible to establish reliably the time dependence of N_2O release relative to the other N-containing species evolved (NO, NO_2 and NH_3). A number of previous studies have indicated that N_2O is formed immediately after the lean to rich transition, and that NH_3 is observed after a slight delay [25,28–30].

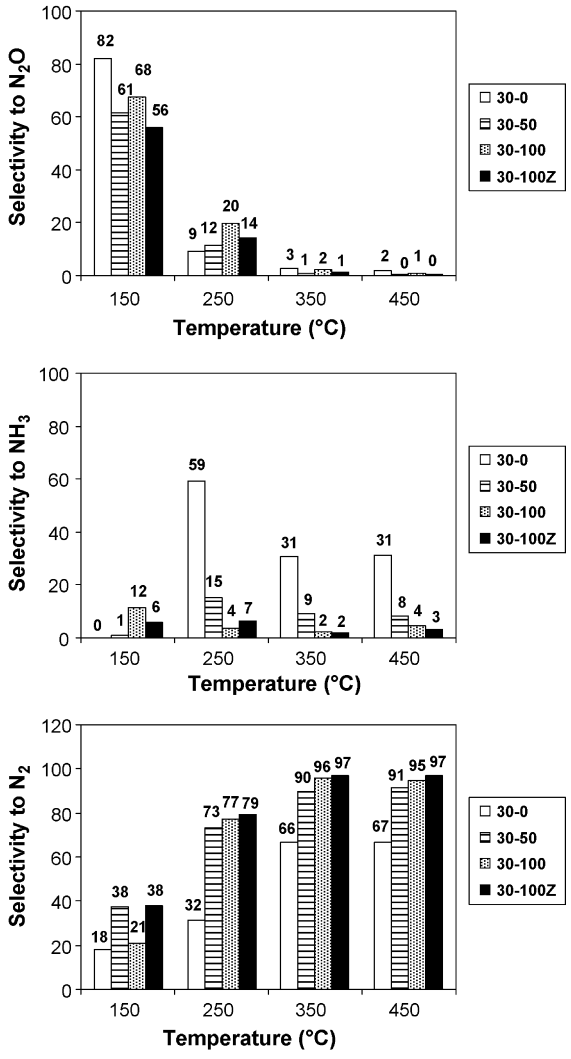

Fig. 5. Selectivity to N_2O (top), NH_3 (middle) and N_2 (bottom) during NO_x reduction under NO_x storage/reduction cycling.

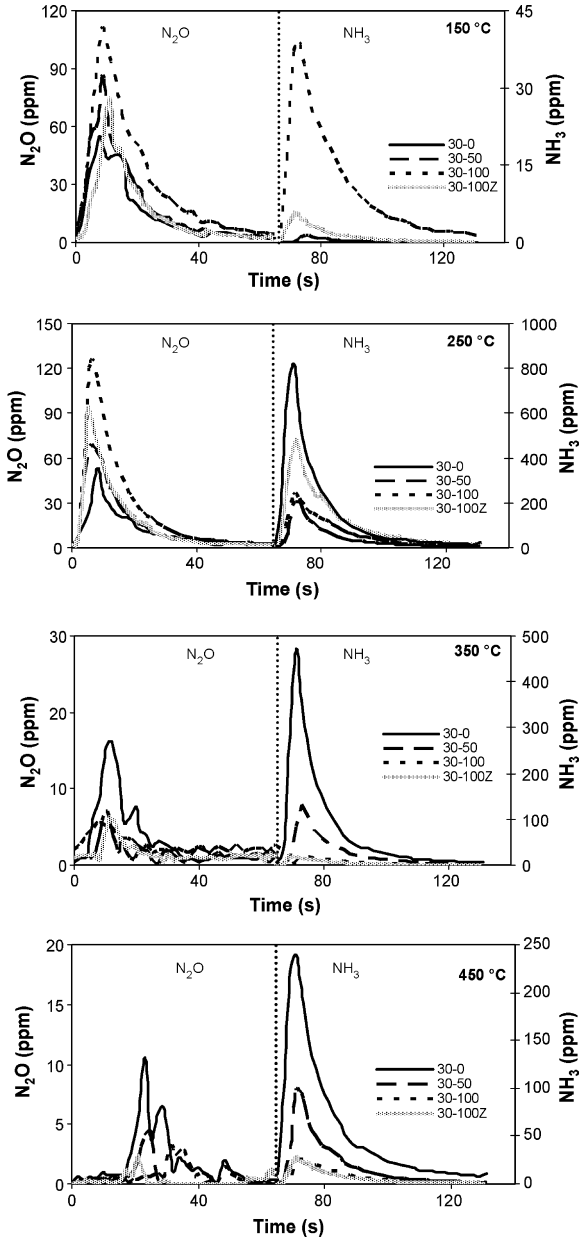

Fig. 6. Evolution of N_2O and NH_3 from catalysts 30–0, 30–50, 30–100 and 30–100 Z during rich phase of NO_x storage/reduction cycling.

With regard to the chemistry of N_2O formation, the results of a recent study by Pihl et al. [31] indicate a number of potential pathways. In the study, NO_x reduction was examined over a commercial LNT catalyst under conditions of continual rich flow and temperature ramping. In experiments using H_2 as the reductant at a 1:1 H_2/NO stoichiometry, N_2O was found to be the dominant reduction product in the 75–150 °C temperature range. At higher H_2/NO stoichiometries (2.5 and 10), NH_3 was the dominant product at 150 °C. When CO was used as the reductant, N_2O was the major product at temperatures up to 200 °C at all stoichiometries examined. While these results indicate that N_2O can be formed at low temperatures as a primary NO_x reduction product, other formation routes are conceivable, such as the reaction of NH_3 with NO_x or the reaction of NH_3 with stored oxygen [31]. In

principle, the reaction of NO with partially reduced ceria constitutes another possible route to N_2O. A previous study has shown that NO can react at surface oxygen vacancies in ceria, with generation of hyponitrite species that decompose with release of N_2O [32]. However, given that the ceria-containing catalysts in this study showed lower selectivity to N_2O than catalyst 30–0 at 150 °C, this route does not appear to play a major role.

Turning to the production of NH_3 over the model catalysts, it is apparent that catalyst ceria content directly impacts the selectivity to NH_3. As shown in Fig. 6, rich phase NH_3 production in the range 250–450 °C, as measured in the reactor effluent, follows the order 30–0 > 30–50 > 30–100 ≈ 30–100 Z. In this context we note that regeneration of a Pt/BaO/Al_2O_3 NO_x trap with H_2 has recently been proposed to occur through the formation of NH_3 as an intermediate [29]. If it is assumed that in the present work NH_3 is initially formed as the main NO_x reduction product, the observed ordering in selectivity can be explained on the basis that as the reaction front propagates along the length of the catalyst, NH_3 formed in situ reacts with oxygen stored in the rear of the catalyst. On this basis, selectivity to NH_3 should decrease with increasing catalyst OSC, as is indeed the case according to our data. We note that NH_3 oxidation by stored oxygen has also been identified as a major pathway for NH_3 consumption in a recently published study in which SpaciMS was used to monitor reactant species in a commercial LNT catalyst [33]. Also of relevance is the report by Pihl et al. [31] that NH_3 oxidation over a commercial LNT affords N_2 as the main product in the range 175–350 °C, NO being the principle product above 350 °C. The latter can be expected to react further with NH_3 during LNT regeneration to afford mainly N_2. Hence these observations are consistent with the notion that for a given set of feed conditions, the ultimate selectivity to NH_3 is largely controlled by the availability of stored oxygen in the catalyst as the reduction front travels along the length of the catalyst.

It is worth noting that an alternative explanation can be formulated to account for the relationship between catalyst ceria content and selectivity to NH_3. If it is assumed that the reaction of stored oxygen with the H_2 and CO reductants results in lower effective reductant concentrations, then a correspondingly lower selectivity to NH_3 should result during NO_x reduction, given that NH_3 formation is favored at high H_2:NO stoichiometries. As shown in Section 3.5 (see below), SpaciMS measurements reveal a net *increase* in the H_2 concentration in the front half of the monolith for catalysts 30–50 and 30–100 (as compared to the inlet H_2 concentration), this being a consequence of the high water–gas shift activity of these catalysts. This result tends to contradict the above explanation, although it must be noted that CO itself can contribute directly to NH_3 formation via isocyanate [34]. Hence, if the net (H_2 + CO):NO ratio were higher for catalyst 30–0 than for 30–50 and 30–100 (even though the H_2:NO ratio is lower), then 30–0 could conceivably produce more NH_3. In the case of 30–100 Z the situation is rather different. As discussed below, the very high OSC of this catalyst results in significant depletion of the reductants and the observation of low intra-catalyst H_2 concentrations. Hence, in this case, effective H_2:NO stoichiometries (and by implication, (H_2 + CO):NO stoichiometries) are indicated to be much lower than for the other catalysts, which should result in decreased NH_3 formation.

Considering the overall selectivity of NO_x reduction (Fig. 5), it is apparent that the ceria-containing catalysts show excellent selectivity to N_2 at 350 and 450 °C. At 150 °C N_2O is the dominant product, although NO_x conversion levels are relatively low, thereby limiting the N_2O yield. At 250 °C, N_2 is the major reduction product, although small amounts of NH_3 and N_2O are also formed. In contrast, catalyst 30–0 shows mediocre selectivity to N_2 at all temperatures. Overall, therefore, these results demonstrate that under the given test conditions ceria incorporation in LNT catalyst formulations is beneficial with respect to the selectivity of NO_x reduction. It should be noted, however, that the reductant concentrations used in this study were chosen to optimize the reduction behavior of catalyst 30–100 Z. If the reductant concentrations were optimized for each catalyst individually (on the basis of catalyst OSC), then different results might be obtained with respect to the NH_3 selectivity. From the preceding discussion, it follows that this would depend on the degree to which NH_3 selectivity is governed by the local (H_2 + CO):NO stoichiometry, as opposed to the idea that it is the availability of stored oxygen in the catalyst which determines the ultimate selectivity to NH_3. This question will be the subject of a future study.

3.5. Intra-catalyst H_2 concentration during rich purging

Ceria has the ability to both catalyze the production of H_2 in situ via the water–gas shift reaction ($CO + H_2O \rightarrow H_2 + CO_2$), and contribute to the consumption of reductants via their reaction with stored oxygen. For this reason, the measurement of intra-catalyst hydrogen concentrations during NO_x reduction was of interest. Fig. 7 shows the results obtained for catalysts 30–0, 30–100 and 30–100 Z under steady state NO_x storage-reduction cycling at 350 °C, the H_2 concentrations being measured at (i) the catalyst inlet (''In Cat''), (ii) one quarter of the way along the catalyst length (''0.25 Cat''), (iii) halfway along the catalyst length (''0.5 Cat''), and (iv) at the catalyst outlet (''Out Cat''). Inspection of the results for catalyst 30–0 reveals a slight increase in the H_2 concentration along the length of the catalyst during the rich phase of the cycling experiment, the outlet H_2 concentration attaining a maximum value of ca. 2.0% (versus the inlet concentration of 1.575%). This finding indicates that catalyst 30–0 possesses activity for the water–gas shift reaction, albeit that the H_2 yield is modest.

In the case of 30–100, the H_2 concentration profiles are rather different. High concentrations of H_2 (up to 3%) are measured at the positions one-quarter and halfway into the catalyst (from the inlet), indicative of high water–gas shift activity. This can be attributed to the presence of the Pt/CeO_2 component, which is known to be a highly active catalyst for this reaction [10,11]. Also of note is the fact that the H_2 concentration measured at the catalyst outlet is very low (<0.5%). This suggests that the H_2 formed is subsequently consumed by reaction with oxygen stored in the rear of the

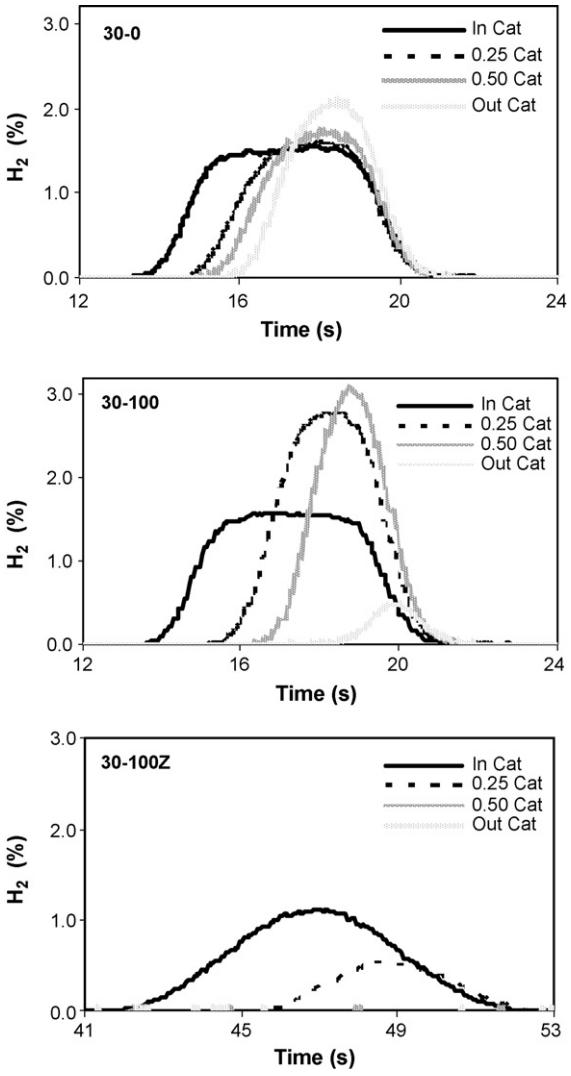

Fig. 7. H_2 concentration profiles measured along the catalyst length during rich purge ($T = 350$ °C).

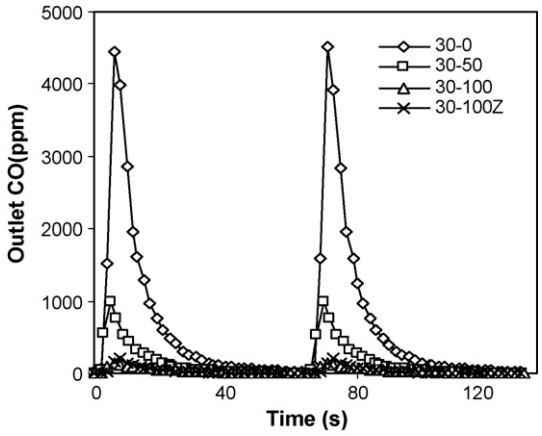

Fig. 8. Outlet CO concentration profiles during rich purge ($T = 350$ °C).

As shown in Fig. 7, the H_2 concentration in the catalyst falls off rapidly from the inlet value, such that no H_2 is detected at the mid-point or in the rear of the catalyst. Coupled with this, the CO concentration measured at the catalyst outlet is found to be near zero for the duration of the rich purge (Fig. 8). These findings suggest that the OSC of the catalyst causes a rapid depletion of the CO and H_2 reductants, although evidently the reductant concentration in the catalyst is sufficient to ensure that a high NO_x conversion level is achieved (97.4%). This, in turn, suggests that the stored NO_x is concentrated in the front part of the catalyst, a conclusion in agreement with several recent studies in which SpaciMS was used to monitor intra-catalyst reactant concentrations during NO_x trap regeneration [21,22].

4. Conclusions

This study has shown that the incorporation of ceria in Ba-based LNT catalysts can significantly influence NO_x storage/reduction performance. Specifically, the following effects were identified:

(i) Under the cycling conditions employed (60 s lean/5 s rich), NO_x storage efficiency in the temperature range 150–350 °C was improved upon addition of ceria to the base Pt/BaO/Al_2O_3 formulation.

(ii) Each of the catalysts displayed lean phase NO_2 slip at 150 °C, indicating that NO oxidation was not rate limiting; rather, NO_x storage at this temperature appears to be limited by the inability to remove nitrates and nitrites during the regeneration phase.

(iii) High rich phase NO_x slip was observed for all of the catalysts at 150 °C, resulting from an imbalance in the rates of nitrate decomposition and NO_x reduction. NO_x slip increased with ceria loading due to the corresponding increase in the amount of NO_x stored. Overall, however, NO_x conversion increased with ceria loading at 150 °C; further, the presence of ceria was found to be beneficial for NO_x conversion across the temperature range 150–350 °C.

(iv) At 450 °C, high rich phase NO_x slip from the most highly loaded ceria-containing catalyst (30–100) resulted in

catalyst, in addition to reaction with the stored NO_x. It can be inferred that towards the rear of the catalyst most of the CO in the feed gas has been consumed (via the water–gas shift reaction, via reaction with stored oxygen and via reaction with stored NO_x), such that the rate of H_2 production from the water–gas shift reaction no longer exceeds the rate of H_2 consumption. FT-IR data are consistent with this idea; as shown in Fig. 8, for catalyst 30–50 the rich phase outlet CO concentration measured during lean–rich cycling does not exceed 0.1% (as compared to the inlet CO concentration of 2.625%), while that for 30–100 is even lower (maximum of 132 ppm). For catalyst 30–0 the rich phase outlet CO concentration is significantly higher (~0.45%), consistent with the observation that the H_2 concentration is still increasing towards the rear of the catalyst (Fig. 7). Hence, the change in outlet CO concentration with ceria content shows the same order as for the outlet H_2 concentration.

For catalyst 30–100 Z very different behavior is observed, resulting from the high OSC of the ceria–zirconia component.

slightly lower total NO_x conversion than the base formulation (30–0). This can be attributed to several factors, including the extremely fast rate of decomposition of cerium nitrates under these conditions, the presence of an exotherm resulting from reaction of the reductants with oxygen stored in the ceria phase, and/or localized reductant shortages at the reaction front due to reductant consumption by stored oxygen (particularly in the rear of the catalyst). This result underscores the need to balance the ceria loading in the catalyst, as noted by Theis et al. [1], particularly with respect to the projected temperature range of operation.

(v) N_2O was the major NO_x reduction product at 150 °C over all of the catalysts, although low NO_x conversion levels limited the N_2O yield. At higher temperatures N_2 was the main product of NO_x reduction, although NH_3 formation was also observed. Selectivity to NH_3 decreased with increasing ceria loading, which is rationalized on the basis that NH_3, formed as a primary reduction product, is consumed by reaction with stored oxygen as the reaction front propagates along the length of the catalyst.

Acknowledgements

The authors thank Eduardo Santillan-Jimenez for TEM measurements, and Dr. Shazam Williams (DCL International Inc.) for helpful discussions. This publication was prepared with the support of the U.S. Department of Energy, under Award No. DE-FC26-05NT42631. However, any opinions, findings, conclusions, or recommendations expressed herein are those of the authors and do not necessarily reflect the views of the DOE.

References

[1] J. Theis, J. Ura, C. Goralski Jr., H. Jen, E. Thanasiu, Y. Graves, A. Takami, H. Yamada, S. Miyoshi, SAE Technical Paper 2003-01-1160, 2003.
[2] E.C. Corbos, S. Elbouazzaoui, X. Cortois, N. Bion, P. Marecot, D. Duprez, Top. Catal. 42/43 (2007) 9.
[3] M. Piacentini, M. Maciejewski, A. Baiker, Appl. Catal. B 72 (2007) 105.
[4] M. Casapu, J.-D. Grunwladt, M. Maciejewski, M. Wittrock, U. Göbel, A. Baiker, Appl. Catal. B 63 (2006) 232.
[5] M. Eberhardt, R. Riedel, U. Göbel, J. Theis, E.S. Lox, Top. Catal. 30/31 (2004) 135.
[6] P. Svedberg, E. Jobson, S. Erkfeldt, B. Andersson, M. Larsson, M. Skoglundh, Top. Catal. 30/31 (2004) 199.
[7] V. Schmeisser, J. de Riva Pérez, U. Tuttlies, G. Eigenberger, Top. Catal. 42/43 (2007) 15.
[8] Y. Ji, T.J. Toops, M. Crocker, Catal. Lett. 119 (2007) 257.
[9] P. Fornasiero, G. Balducci, R. Di Monte, J. Kaspar, V. Sergo, G. Gubitosa, A. Ferrero, M.J. Graziani, J. Catal. 164 (1996) 173.
[10] A.A. Phatak, N. Koryabkina, S. Rai, J.L. Ratts, W. Ruettinger, R.J. Farrauto, G.E. Blau, W.N. Delgass, F.H. Ribeiro, Catal. Today 123 (2007) 224.
[11] G. Jacobs, L. Williams, U. Graham, D.E. Sparks, B.H. Davis, Appl. Catal. A 252 (2003) 107.
[12] M. Haneda, T. Morita, Y. Nagao, Y. Kintaichi, H. Hamada, Phys. Chem. Chem. Phys. 3 (2001) 4696.
[13] Y. Ji, T.J. Toops, G. Uschi, G. Jacobs, M. Crocker, Catal. Lett. 110 (2006) 29.
[14] S. Philipp, A. Drochner, J. Kunert, H. Vogel, J. Theis, E.S. Lox, Top. Catal. 30/31 (2004) 235.
[15] M.O. Symalla, A. Drochner, H. Vogel, S. Philipp, U. Göbel, W. Müller, Top. Catal. 42/43 (2007) 199.
[16] E. Rohart, V. Bellière-Baca, K. Yokota, V. Harlé, C. Pitois, Top. Catal. 42/43 (2007) 71.
[17] B. Adelman, Report Prepared for the Coordinating Research Council, CRC Project No. AVFL-7, June 2002, Available at: http://www.crcao.-com/reports/recentstudies00-02/AVFL-7FinalReport.pdf.
[18] T. Morita, N. Suzuki, N. Satoh, K. Wada, H. Ohno, SAE Technical Paper 2007-01-0239, 2007.
[19] W.P. Partridge, J.M.E. Storey, S.A. Lewis, R.W. Smithwick, G.L. DeVault, M.J. Cunningham, N.W. Currier, T.M. Yonushonis, SAE Technical Paper 2000-01-2952, 2000.
[20] B.H. West, S.P. Huff, J.E. Parks, S.A. Lewis, J.-S. Choi, W.P. Partridge, J.M. Storey, SAE Technical Paper 2004-01-3023, 2004.
[21] J.-S. Choi, W.P. Partridge, C.S. Daw, Appl. Catal. A 293 (2005) 24.
[22] J.-S. Choi, W.P. Partridge, W.S. Epling, N.W. Currier, T.M. Yonushonis, Catal. Today 114 (2006) 102.
[23] C.E. Hori, H. Permana, K.Y.S. Ng, A. Brenner, K. More, K.M. Rahmoeller, D. Belton, Appl. Catal. B 16 (1998) 105.
[24] X. Chen, J. Schwank, J. Li, W.F. Schneider, C.T. Goralski Jr., P.J. Schmitz, Appl. Catal. B 61 (2005) 164.
[25] W.S. Epling, A. Yezerets, N.W. Currier, Appl. Catal. B 74 (2007) 117.
[26] L. Yang, O. Kresnawahjuesa, R.J. Gorte, Catal. Lett. 72 (2000) 33.
[27] J.R. Theis, J.A. Ura, J.J. Li, G.G. Surnilla, J.M. Roth, C.T. Goralski Jr., SAE Technical Paper 2003-01-1159, 2003.
[28] R.G. Tonkyn, R.S. Disselkamp, C.H.F. Peden, Catal. Today 114 (2006) 94.
[29] L. Cumaranatunge, S.S. Mulla, A. Yezerets, N.W. Currier, W.N. Delgass, F.H. Ribeiro, J. Catal. 246 (2007) 29.
[30] L. Castoldi, I. Nova, L. Lietti, P. Forzatti, Catal. Today 96 (2004) 43.
[31] J.A. Pihl, J.E. Parks II, C.S. Daw, T.W. Root, SAE Technical Paper 2006-01-3441, 2006.
[32] A. Martínez-Arias, J. Soria, J.C. Conesa, X.L. Seoane, A. Arcoya, R. Cataluna, J. Chem. Soc. Faraday Trans. 91 (1995) 1679.
[33] J. Parks II., S. Huff, M. Swartz, B. West, Presentation at 10th CLEERS Workshop, Dearborn, MI, May 2, 2007.
[34] T. Szailer, J.H. Kwak, D.H. Kim, J.C. Hanson, C.H.F. Peden, J. Szanyi, J. Catal. 239 (2006) 51.